Testing General Relativity Using Galileo Satellite Signals

Gabriele Giorgi, Martin Lülf, and Christoph Günther
Institute for Communications and Navigation
Technische Universität München
Munich, Germany
Emails: gabriele.giorgi@tum.de, martin.luelf@tum.de, christoph.guenther@tum.de

Sven Herrmann, Daniela Kunst, Felix Finke, and Claus Lämmerzahl
Center for Applied Space Technology and Microgravity (ZARM)
University of Bremen
Bremen, Germany
Emails: sven.herrmann@zarm.uni-bremen.de, daniela.kunst@zarm.uni-bremen.de, felix.finke@zarm.uni-bremen.de, claus.laemmerzahl@zarm.uni-bremen.de

***Abstract*—The two Galileo satellites launched in 2014 (E14 and E18) were injected in orbits with a significant eccentricity. Both the gravitational potential at the location of the satellites and their velocity thus change as a function of time. Since the Galileo satellites carry very stable clocks, these can potentially be used to set new bounds to the level of agreement between measurements of the clocks' frequency shifts and their prediction by the theory of relativity. This paper presents some initial results obtained by processing available data from Galileo satellite E18.**

I. Motivation

The first two satellites part of the Full Operational Capability (FOC) phase of the Galileo program (identified with codes E14 and E18) were injected into orbits with an eccentricity of 0.29. This eccentricity was later reduced to about 0.16 with several orbital maneuvers, but it is still much larger than the nominal value of 0.0002. A further reduction was not possible due to the limited amount of fuel onboard the satellites. The European Space Agency (ESA) is presently (2016) assessing whether the two satellites can still be integrated in standard operations. On the other hand, the higher eccentricity is an opportunity for science. The two satellites are transmitting navigation signals timed by one of the four onboard stable atomic clocks: two Rubidum clocks and two passive Hydrogen Masers (HMs). The former are characterized by an Allan standard deviation $\sigma = 2 \cdot 10^{-14}$ at $2.5 \cdot 10^4$s [1], the latter are even more stable, at $\sigma = 7 \cdot 10^{-15}$ at 10^4s [2]. The high stability of these clocks provides an excellent opportunity for a space-based experimental test of general relativity. The long term availability of measurements allows to successively reduce the statistical uncertainty.

According to general relativity, the rate of a clock located at a position of higher gravitational potential is increased when compared to a clock situated in a region of lower gravitational potential. This is commonly known as the gravitational redshift and it has been experimentally tested in the Vessot-Levine rocket experiment Gravity Probe A (GP-A) in 1976 to an accuracy of 1.4×10^{-4} [3]-[4].

In this work we study the relativistic offset (redshift and Doppler shift) of the HM clock onboard the Galileo satellite E18 with respect to a reference atomic clock on Earth. The eccentric orbit enables a comparison of the rate of the clocks at different gravitational potentials repeatedly. The high stability of the onboard atomic clocks and potentially long observation spans reduce the statistical uncertainty of the estimates, thus enabling measurements of the gravitational redshift with a high level of accuracy [5], provided that all systematic errors are correctly accounted for.

II. Relativistic effects

Ashby [6] derives the following metric in the Earth-Centered-Inertial (ECI) frame:

$$ds^2 = \left(1 + \frac{2\left(V - \Phi_\oplus\right)}{c^2}\right)(cdt)^2 - \left(1 - \frac{2V}{c^2}\right)\left(dr^2 + r^2 d\Omega^2\right) , \tag{1}$$

where c is the speed of light; V is the Newtonian gravitational potential of the Earth, approximately given by

$$V = -\frac{GM_\oplus}{r}\left(1 - J_2\left(\frac{a_\oplus}{r}\right)^2 P_2(\sin\theta)\right) , \tag{2}$$

with $J_2 = 1.08263 \times 10^{-3}$ the Earth's quadrupole moment coefficient (we will keep the assumption of small $\frac{V}{c^2}$ throughout this manuscript), $a_\oplus = 6.3781370 \times 10^6$ m the Earth's equatorial radius, and P_2 the Legendre polynomial of degree 2; $\Phi_\oplus$ is the effective gravitational potential of the Earth on the geoid (WGS-84) [7] in the rotating frame, which includes a $1/r$ contribution due to the Earth's mass, a contribution from the quadrupole potential, and a centripetal contribution due to the Earth's rotation (a reference value is defined by the Astronomical Union as $\frac{\Phi_\oplus}{c^2} = -6.969290134 \times 10^{-10}$); t is the coordinate time – defined by the rate of reference clocks at rest located on Earth's geoid; $d\Omega^2 = d\theta^2 + \sin(\theta)^2 d\phi^2$ is the two dimensional angular line element; and (r, θ, ϕ) are the spherical polar coordinates. It can be easily verified that the proper time of a clock located on the Earth's geoid is equal to the coordinate time t, so that it may serve as the correct

978-0-9928-6265-7/16/$31.00 ©2016 IEEE

basis for synchronization. This provides the foundation for the comparison of satellite clock rates in different gravitational potentials. Using the metric given in Eq. (1), the proper time increment of a clock moving with velocity v in the gravitational field is computed as

$$d\tau_{\rm sat} = \left(1 + \frac{(V - \Phi_\oplus)}{c^2} - \frac{v^2}{2c^2}\right) dt \ . \tag{3}$$

The second term on the right-hand side $\frac{(V-\Phi_\oplus)}{c^2}$ represents the contribution from the gravitational redshift due to the difference in the gravitational potential. Since it enters with a positive sign, this term describes the advance of the satellite's clock with respect to the reference clock on Earth. The third term ($\frac{v^2}{2c^2}$) corresponds to the contribution from special relativity – the second-order Doppler effect – which enters with a negative sign, implying the dilation of time of the moving clock. Integration along the path of the satellite's clock yields the elapsed proper time

$$\Delta\tau_{\rm sat} = \Delta t + \int\limits_{\rm path} \left(\frac{(V - \Phi_\oplus)}{c^2} - \frac{v^2}{2c^2}\right) dt \ . \tag{4}$$

Thus, the relativistic correction to be applied to a satellite clock orbiting the Earth amounts to

$$\begin{aligned} \Delta_{\rm rel} &= \Delta\tau_{\rm sat} - \Delta t \\ &= \int\limits_{\rm path} \left(\frac{(V - \Phi_\oplus)}{c^2} - \frac{v^2}{2c^2}\right) dt \ . \end{aligned} \tag{5}$$

Assume the path of the satellite to be an elliptic Kepler orbit so that the radial distance is given by the Keplerian orbital parameters

$$r = a\left(1 - e\cos\left(E\right)\right) \ , \tag{6}$$

where a is the semi-major axis, e is the eccentricity and E is the eccentric anomaly. Using the orbital energy conservation equation

$$\frac{v^2}{2} - \frac{GM_\oplus}{r} = -\frac{GM_\oplus}{2a} \ , \tag{7}$$

the velocity term in Eq. (4) can be substituted with (7), obtaining

$$\Delta_{\rm rel} = \int\limits_{\rm path} \left(-\left(\frac{3GM_\oplus}{2ac^2} + \frac{\Phi_\oplus}{c^2}\right) + \frac{2GM_\oplus}{c^2}\left(\frac{1}{a} - \frac{1}{r}\right)\right) dt \ . \tag{8}$$

The first term on the right-hand side is of linear order in time, and corresponds to a constant frequency offset. This offset is usually factory-adjusted on navigation satellites before launch, by accordingly reducing the nominal transmitting frequency [6]. The second term describes the modulated component of both the gravitational redshift and the second-order Doppler effects. While this modulation is of limited amplitude ($\approx \pm 0.5$ ns) for Galileo satellites moving on nominal orbits ($e = 0.0002$), the higher eccentricity of the orbits of satellites E14 and E18 increases the amplitude to approximatively 370 ns. This large contribution provides us with a good opportunity to perform highly precise observations of the gravitational redshift using the atomic clocks onboard E14 and E18.

III. Galileo satellites

Galileo FOC satellites transmit three independent Code Division Multiple Access (CDMA) signals, named E1, E5 and E6. All signals are Right-Hand Circularly Polarized (RCHP) [8]. Six signals are accessible to all Galileo users on the E1 and E5 bands for Open Services (OS), whereas four additional signals on E1 and E6 bands are only accessible to authorized users for Commercial Services (CS) and Public Regulated Services (PRS). In the remainder of this manuscript, we only refer to the OS signals in the E1 and E5 bands, and more specifically the E1 and E5a signals.

Three main types of measurements are available: pseudorange, carrier-phase, and Doppler. Pseudorange measurements are derived by multiplying the speed of light with the signal time-of-flight. The prefix *pseudo* is attached to stress that the actual measurement deviates from the theoretical geodesic due to a number of systematic effects (e.g., synchronization biases, perturbations introduced by the atmosphere, antenna effects, multipath) and inherent measurement noise. The fractional carrier phase and the Doppler measurements are extracted from the carrier tracking loop. The noise of carrier phase measurements is two orders of magnitude smaller than for pseudorange measurements. Unfortunately, carrier phase measurements are affected by an integer ambiguity, due to the 2π-periodicity of the carrier phase. These ambiguities must be removed in order to fully exploit the higher precision of the carrier phase observations.

If the position of both a receiver on Earth and a transmitting satellite are precisely known, the pseudorange and carrier-phase measurements can be used to assess the timing differential between the orbiting clock and the clock at rest on Earth. This differential is produced by a number of contributing factors, which can be classified within three segments: satellite (antenna, clock bias and errors, linear and rotational motion), propagation (ionospheric and tropospheric delays) and receiver (antenna, clock bias and errors, multipath) contributes. Clock biases due to relativistic effects, caused by both the relative motion and the gravitational differential between satellite and reference clocks, constitute the largest factor for satellites on orbits with non-negligible eccentricities. Observations from Galileo satellites E14 and E18 (cf. Table I) show a time-dependent bias with one-orbit period and an amplitude of about 370 ns (cf. section II).

IV. Handling of Galileo data

The pseudorange and carrier-phase observations measured by a receiver r tracking satellite s at coordinate time t on

TABLE I
ORBITAL PARAMETERS OF GALILEO SATELLITES E14 AND E18 ON DAY 252 (2015).

	E14	E18
Semi-major axis a [Km]	27977	27978
Eccentricity e	0.157	0.157
Inclination i [deg]	49.926	49.869
Height at apogee [Km]	26002	26004
Height at perigee [Km]	17207	17205
Orbital period [h]	12.94	12.94

channel (frequency) f are modeled as [9]

$$\begin{aligned} P^s_{r,f}(t) &= \|\mathbf{r}_r(t) - \mathbf{r}^s(t-T)\| + c(\Delta t_r(t) - \Delta t^s(t-T)) \\ &\quad + c(d_{r,f}(t) - d^s_f(t-T)) + \mathcal{I}^s_{r,f}(t) + \mathcal{T}^s_r(t) \\ &\quad + \mathrm{m}^s_{r,P,f}(t) + \epsilon^s_{r,P,f}(t)\ , \\ \lambda_f \Phi^s_{r,f}(t) &= \|\mathbf{r}_r(t) - \mathbf{r}^s(t-T)\| + c(\Delta t_r(t) - \Delta t^s(t-T)) \\ &\quad + c(\delta_{r,f}(t) - \delta^s_f(t-T)) - \mathcal{I}^s_{r,f}(t) + \mathcal{T}^s_r(t) \\ &\quad + \mathrm{m}^s_{r,\Phi,f}(t) + \lambda_f(\phi^s_{r,f}(t_0) - \phi^s_f(t_0)) + \lambda_f N^s_{r,f} \\ &\quad + \lambda_f \Delta\varphi^s_r(t-t_0) + \epsilon^s_{r,\Phi,f}(t)\ , \end{aligned} \tag{9}$$

with

P	pseudorange measurement [m]
Φ	carrier phase measurement [cycles, fractional]
T	signal satellite-to-receiver travel time [s]
t_0	time of reference for phase synchronization [s]
$\mathbf{r}^s, \mathbf{r}_r$	satellite and receiver vectorial position [m]
$\mathcal{I}$, $\mathcal{T}$	ionospheric and tropospheric delays [m]
m	multipath error [m]
c	speed of light : 299 792 458 [m/s]
Δt	clock biases [s]
d , δ	instrumental delays [s]
ϕ	phase of the generated carrier signal (original or replica) [cycles]
λ_f	signal wavelength at frequency f [m]
N	number of complete carrier phase cycles that have occurred between signal generation and signal carrier phase measurement [integer cycles]
$\Delta\varphi^s_r$	phase wind-up [cycles, fractional]
ϵ_P , ϵ_Φ	remaining unmodeled pseudorange and carrier phase errors [m]

The range between satellite and receiver $\|\mathbf{r}_r(t) - \mathbf{r}^s(t-T)\|$ refers to the geometrical distance between the respective antenna phase centers. Atmosphere-induced delays are accounted for in the ionospheric ($\mathcal{I}$) and tropospheric ($\mathcal{T}$) delay terms, expressed in meters. The effect of the non-perfect time synchronization of both receiver and satellite clocks is captured by the clock bias terms Δt, i.e., the clocks' offset from the coordinate time. d and δ denote the pseudorange and carrier-phase instrumental delays, respectively. These delays can be frequency-dependent. The measurements are also affected by undesired replicas of the incoming signal, whose contributes are lumped in terms m_P and m_Φ, indicating the pseudorange and carrier phase multipath errors, respectively. The carrier phase observations Φ are ambiguous by an integer number of full cycles, denoted with N. Finally, the phase variation due to the slow rotation of the transmitting satellite – the phase wind-up effect – is modeled and denoted with $\Delta\varphi^s_r(t-t_0)$.
We assume the presence of zero-mean additive noise on both pseudorange and carrier phase measurements, with variances (constant across all channels) σ^2_P and σ^2_Φ, respectively [10]. An elevation-dependent model is applied to down-weight observations when the satellite is at low elevation [11]:

$$\sigma^2_{P/\Phi,w}(t) = \sigma^2_{P/\Phi}\left(1 + 10e^{-\frac{\theta^s(t)}{\theta_c}}\right)\ , \tag{10}$$

with $\theta^s(t)$ the satellite elevation at time t and θ_c the cut-off angle (observations from satellites whose elevation is lower than the cut-off angle are discarded).
The differential clock bias $\Delta t^s_r(t,T) = \Delta t_r(t) - \Delta t^s(t-T)$ can be decomposed in three main constituents:

$$\Delta t^s_r(t,T) = \Delta t^s_{r,I}(t,T) + \Delta t^s_{r,II}(t,T) + \Delta t^s_{r,\mathrm{III}}(t,T)\ . \tag{11}$$

The three terms in (11) describe the inherent (constant, linear and second-order terms in time) bias and drift of receiver and satellite clocks ($\Delta t^s_{r,I}$), the (linear) drift due to the constant-rate components in the relativistic correction term in (8) ($\Delta t^s_{r,II}$), and a modulated signal due to the combined effect of second-order Doppler shift and gravitational redshift ($\Delta t^s_{r,III}$). The latter is the signal of interest for the scope of this work.

A. The International GNSS Service products

The International GNSS Service (IGS) is a voluntary federation of a number of institutions spanning the whole globe, which aims at providing very high precision products in support of scientific uses of GNSSs. IGS products include GNSS satellite ephemerides, Earth rotation parameters, global tracking station coordinates and velocities, satellite and tracking station clock information, zenith tropospheric path delay estimates, and global ionosphere maps. These products are obtained from a global tracking network of more than 300 permanent, continuously-operating GNSS stations that provide a large data set to a number of IGS analysis centers (ACs). Currently, the IGS only officially releases GPS and GLONASS data, but a Multi-GNSS Experiment (MGEX) has been active since 2011 to track, process and analyze all available GNSS signals, including those from Galileo satellites. The harmonization and collective contribute of each GNSS will allow for more precise products, especially with respect to atmospheric parameters [12], [13]. Several MGEX-ACs, such as TUM (Technische Universität München) or CODE (Center for Orbit Determination in Europe), make available products relative to Galileo satellites E14 and E18 (since 2015). For our scopes, accurate and unbiased products are paramount. Any bias that is systematically modulated with one-orbit period is detrimental to the precision of the gravitational redshift measurements. The accuracy of the available satellite orbit is the main limiting factor for a precise measurement of the gravitational redshift.

TABLE II
ACCURACY OF CODE PRODUCTS

Product	Accuracy
Orbit [17]	15 cm
Station coordinates [15]	3 mm (Horizontal)
	6 mm (Vertical)
Receiver clock	0.05 ns
Troposphere zenith delay [18]	5 mm

B. Extracting the relativistic signature

For a first analysis, pseudorange and carrier phase observations from the Geodetical Observatory Wettzell, Germany (WTZ3) are used. The geometric range between receiver and satellite is computed using the daily station coordinates and the satellite orbit from CODE. We also use the station clock correction and the tropospheric zenith delays from CODE. The latter delays are mapped to tropospheric slant delays $\mathcal{T}_r^s$ using the Niell mapping function [14]. The satellite and receiver antenna phase center offsets are compensated by using the conventional IGS calibration data [15]. Finally, the phase wind-up is removed by applying a nominal attitude model [16]. The observation model for measurements in the E1- and E5a-band after corrections reads

$$\begin{aligned} P'_{E1}(t) &= c\Delta t(t,T) + \mathcal{I}_{E1}(t) + \varepsilon'_{P,E1}(t) \ , \\ P'_{E5}(t) &= c\Delta t(t,T) + \mathcal{I}_{E5}(t) + \varepsilon'_{P,E5}(t) \ , \\ \lambda_{E1}\Phi'_{E1}(t) &= c\Delta t(t,T) - \mathcal{I}_{E1}(t) + \lambda_{E1}L_{E1} + \varepsilon'_{\Phi,E1}(t) \ , \\ \lambda_{E5}\Phi'_{E5}(t) &= c\Delta t(t,T) - \mathcal{I}_{E5}(t) + \lambda_{E5}L_{E5} + \varepsilon'_{\Phi,E5}(t) \ , \end{aligned} \tag{12}$$

where we dropped the sub- and superscripts denoting receiver and satellite, and we lumped the fractional and integer phase terms into the real-valued parameter L. Neither instrumental delays, nor multipath, are modeled. The remaining parameters can then be estimated with an accuracy proportional to the available CODE products summarized in Table II [15]-[17]-[18]. Note that the use of external products may introduce undesired systematic effects [19]. The accuracy of the applied corrections is dominated by the satellite's orbit accuracy. Using dual frequencies observations, no external ionosphere model is necessary: the first-order ionospheric delay can be estimated by relating the delay on the two signals with [9]

$$\mathcal{I}_{E5}(t) = \frac{f_{E1}^2}{f_{E5}^2}\mathcal{I}_{E1}(t) \ . \tag{13}$$

Higher-order ionospheric delays – up to 2 cm [20] – remain uncompensated. This leaves one time-dependent clock term, one time-dependent ionospheric term and two constant real-valued ambiguity terms to be estimated over m epochs of measurements. We can then write the following observation model for casting observations from m epochs:

$$\mathbf{y} = \mathbf{A}\mathbf{x} \ , \tag{14}$$

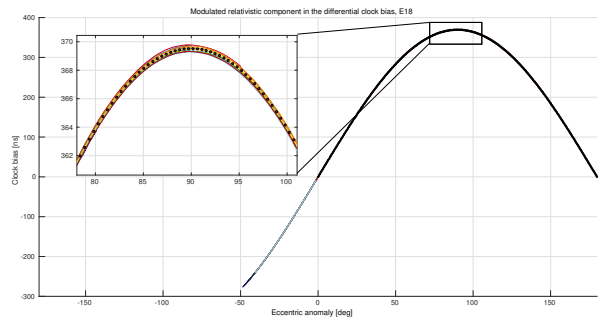

Fig. 1. Epoch-by-epoch estimated (for 51 arcs above the reference station) and theoretical (red dots) modulated component of the relativistic signature, as function of the satellite orbital position.

with

$$\begin{aligned} \mathbf{y} &= \left(\mathbf{y}_{P'_{E1}} \ , \ \mathbf{y}_{P'_{E5}} \ , \ \mathbf{y}_{\Phi'_{E1}} \ , \ \mathbf{y}_{\Phi'_{E5}}\right)^{\mathrm{T}} \ , \\ \mathbf{x} &= (c\boldsymbol{\Delta}\mathbf{t}^{\mathrm{T}} \ , \ \boldsymbol{\mathcal{I}}^{\mathrm{T}} \ , \ \mathbf{L}^{\mathrm{T}})^{\mathrm{T}} \ , \\ \boldsymbol{\Delta}\mathbf{t} &= (\Delta t(t_1,T) \ , \ \ldots \ , \ \Delta t(t_m,T))^{\mathrm{T}} \ , \\ \boldsymbol{\mathcal{I}} &= (\mathcal{I}_{E1}(t_1) \ , \ \ldots \ , \ \mathcal{I}_{E1}(t_m))^{\mathrm{T}} \ , \\ \mathbf{L} &= (L_{E1} \ , \ L_{E5})^{\mathrm{T}} \ , \\ \mathbf{A} &= \begin{bmatrix} \mathbf{I}_m & \mathbf{I}_m & \mathbf{0} & \mathbf{0} \\ \mathbf{I}_m & \frac{f_{E1}^2}{f_{E5}^2}\mathbf{I}_m & \mathbf{0} & \mathbf{0} \\ \mathbf{I}_m & -\mathbf{I}_m & \lambda_{E1}\mathbf{e}_m & \mathbf{0} \\ \mathbf{I}_m & -\frac{f_{E1}^2}{f_{E5}^2}\mathbf{I}_m & \mathbf{0} & \lambda_{E5}\mathbf{e}_m \end{bmatrix} . \end{aligned} \tag{15}$$

$\mathbf{I}_m$ denotes the $m \times m$ identity matrix and $\mathbf{e}_m$ denotes an m-vector of ones. Each vector $\mathbf{y}_{P'_f/\Phi'_f}$ in $\mathbf{y}$ casts the m corrected pseudorange or carrier phase measurements at frequency f (cf. Eq.12).

The variance-covariance (v-c) matrix $\mathbf{Q}_{\mathbf{yy}}$ that characterizes the measurement dispersion is built as

$$\mathbf{Q}_{\mathbf{yy}} = \mathrm{diag}\left(\mathbf{Q}_{\mathbf{P}_{E1}}, \mathbf{Q}_{\mathbf{P}_{E5}}, \mathbf{Q}_{\boldsymbol{\Phi}_{E1}}, \mathbf{Q}_{\boldsymbol{\Phi}_{E5}}\right) \ , \tag{16}$$

with

$$\begin{aligned} \mathbf{Q}_{\mathbf{P}_{E1}} &= \mathrm{diag}\left(\sigma^2_{P_{E1},w}(t_1), \ldots, \sigma^2_{P_{E1},w}(t_m)\right) \ , \\ \mathbf{Q}_{\mathbf{P}_{E5}} &= \mathrm{diag}\left(\sigma^2_{P_{E5},w}(t_1), \ldots, \sigma^2_{P_{E5},w}(t_m)\right) \ , \\ \mathbf{Q}_{\boldsymbol{\Phi}_{E1}} &= \mathrm{diag}\left(\sigma^2_{\Phi_{E1},w}(t_1), \ldots, \sigma^2_{\Phi_{E1},w}(t_m)\right) \ , \\ \mathbf{Q}_{\boldsymbol{\Phi}_{E5}} &= \mathrm{diag}\left(\sigma^2_{\Phi_{E5},w}(t_1), \ldots, \sigma^2_{\Phi_{E5},w}(t_m)\right) \ , \end{aligned} \tag{17}$$

and $\sigma_{P_{E1}} = \sigma_{P_{E5}} = 0.5$ m and $\sigma_{\Phi_{E1}} = \sigma_{\Phi_{E5}} = 0.005$ m. Expressions (14) and (16) define the functional and stochastic models used. The least-squares adjustment reads

$$\begin{aligned} \hat{\mathbf{x}} &= (\mathbf{A}^{\mathrm{T}}\mathbf{Q}_{\mathbf{yy}}^{-1}\mathbf{A})^{-1}\mathbf{A}^{\mathrm{T}}\mathbf{Q}_{\mathbf{yy}}^{-1}\mathbf{y} \ , \\ \mathbf{Q}_{\hat{\mathbf{x}}\hat{\mathbf{x}}} &= (\mathbf{A}^{\mathrm{T}}\mathbf{Q}_{\mathbf{yy}}^{-1}\mathbf{A})^{-1} \ . \end{aligned} \tag{18}$$

Note that both the differential clock bias and the ionospheric delay terms are estimated epoch-by-epoch. The differential clock biases after removing the satellite constant, linear and second-order drift with a second-order polynomial fitting are visualized for 51 passages over the Wettzel reference station in

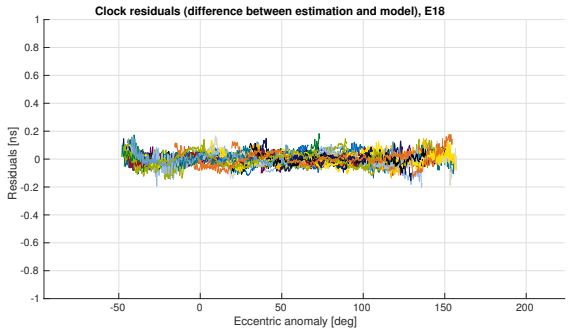

Fig. 2. Epoch-by-epoch (30 seconds samples) difference between estimated and theoretical relativistic signature as function of the satellite orbital position.

Fig. 1: the modulated component due to the combined effects of gravitational redshift and second-order Doppler shows a good fit with the prediction from model (8). Fig. 2 visualizes the difference between the data and model for the 51 arcs analyzed: the residual noise and systematic effects are within a fraction of a nanosecond.

V. Conclusions and further work

This work focused on analyzing the opportunity offered by Galileo satellites E14 and E18 to test the gravitational redshift. Thanks to the eccentric orbits and the availability of highly stable atomic clocks onboard both satellites, a precise observation of the relative time offset between clocks on Earth and the two orbiting clocks is and will be available over a large time span, enabling a prolonged space-based test of the gravitational redshift predicted within the framework of general relativity. Aiming at improving on the current accuracy in the measurement of the gravitational redshift effect (cf. section II), presently at 140 ppm [4], a joint project by the Institute of Communication and Navigation (Technische Universität München) and the Center for Applied Space Technology and Microgravity (University of Bremen) will focus on analyzing and mitigating any remaining spurious contributes in the estimation of the differential clock bias. In order to refine the estimation process, an improved orbit determination scheme including ad-hoc solar and thermal radiation pressure parameters [21]-[22] and a satellite clock model will be applied, reducing any systematic effect associated to the satellite orbit and clock terms. Furthermore, larger time spans from multiple reference stations will be processed, contributing to reduce the measurement noise and augmenting both the availability and the statistical meaning of the data.

Acknowledgment

This project is supported by the German Space Agency (DLR) with funds provided by the Federal Ministry for Economic Affairs and Energy (BMWi) due to an enactment of the German Bundestag under grant numbers FKZ 50WM1547/1548 (RELAGAL, Test of RELAtivity theory with GALileo satellites). The support of Hansjörg Dittus (DLR) and Fritz Merkle (OHB) was greatly appreciated.

References

[1] P. Rochat, F. Droz, P. Mosset, G. Barmaverain, Q. Wang, D. Boving, L .Mattioni, M. Belloni, M. Gioia, U. Schmidt, T. Pike, F. Emma, "The Onboard Galileo Rubidium and Passive Maser, Status & Performance," *Proc. IEEE Int. Freq. Contr. Symp. and Exp.,* pp. 26–32, 2005.

[2] L. Mattioni, M. Belloni, P. Berthoud, I. Pavlenko, H. Schweda, Q. Wang, P. Rochat, F.Droz, P. Mosset, H. Ruedin, "The Development of a Passive Hydrogen Maser Clock for the Galileo NavigationSystem," *34th PTTI Meet.,* pp. 161–170, 2002.

[3] R.F.C. Vessot, and M.W. Levine, "A test of the equivalence principle using a space-borne clock," *General Relativity and Gravitation*, 10, pp. 181–204, 1979.

[4] R.F.C. Vessot, "Clocks and spaceborne tests of relativistic gravitation," *Advances in Space Research*, 9, pp. 21–28, 1989.

[5] P. Delva, A. Hees, S. Bertone, E. Richard and P. Wolf, "Test of the gravitational redshift with stable clocks in eccentric orbits: application to Galileo satellites 5 and 6," *Classical and Quantum Gravity*, 32, 232003, 2015.

[6] N. Ashby, "Relativity in the Global Positioning System," *Living Reviews in Relativity*, 6, 1, 2003.

[7] "World Geodetic System 1984, Its Definition and Relationships With Local Geodetic Systems," *NIMA Technical Report TR8350.2*, Third Edition, 1997.

[8] European Union, "European GNSS (Galileo) open service: signal in space interface control document," *Luxembourg, Publications Office of the European Union*, 2nd rev., 2015.

[9] A. Kleusberg, and P.J.G. Teunissen, "GPS for Geodesy," Springer-Verlag, 1996.

[10] C.C.J.M. Tiberius, and K. Borre, "Are GPS data normally distributed?," *in Schwartz, Klaus-Peter (ed.), Geodesy Beyond 2000 : the Challenges of the First Decade. IAG General Assembly*, 121, pp. 245–248, 2000.

[11] H.J. Euler, and C.C. Goad, "On optimal filtering of GPS dual frequency observations without using orbit information," *Bulletin Géodésique*, 65(2), pp. 130–143, 1991.

[12] J.M. Dow, R.E. Neilan, and C. Rizos, "The International GNSS Service in a changing landscape of Global Navigation Satellite Systems," *Journal of Geodesy*, 83(3-4), pp. 191–198, 2009.

[13] O. Montenbruck, P. Steigenberger, R. Khachikyan, G. Weber, R.B. Langley, L. Mervart, and U. Hugentobler, "IGS-MGEX: Preparing the Ground for Multi-Constellation GNSS Science," *InsideGNSS*, 9(1), pp. 42–49, 2014.

[14] A.E. Niell, "Global mapping functions for the atmosphere delay at radio wavelengths," *Journal of Geophysical Research*, 101(B2), pp. 3227–3246, 1996.

[15] R. Ferland, and M. Piraszewski, "The IGS-combined station coordinates, earth rotation parameters and apparent geocenter," *Journal of Geodesy*, 83(3), pp. 385–392, 2009.

[16] J. Wu, S. Wu, G. Hajj, W. Bertiguer, and S. Lichten, "Effects of Antenna Orientation on GPS Carrier Phase Measurements," *Manuscripta Geodaetica*, pp. 91–98, 1993.

[17] P. Steigenberger, U. Hugentobler, S. Loyer, F. Perosanz, L. Prange, R. Dach, M. Uhlemann, G. Gendt, and O. Montenbruck, "Galileo Orbit and Clock Quality of the IGS Multi-GNSS Experiment," *Advances in Space Research*, 55(1), pp. 269–281, 2015.

[18] S.H. Byun, and Y.E. Bar-Sever, "A new type of troposphere zenith path delay product of the international GNSS service," *Journal of Geodesy*, 83(3), pp. 1–7, 2009.

[19] O. Montenbruck, P. Steigenberger, and U. Hugentobler, "Enhanced Solar Radiation Pressure Modeling for Galileo Satellites," *Journal of Geodesy*, 89(3), pp. 283–297, 2015.

[20] M. Hernndez-Pajares, J.M. Juan, J. Sanz, and R. Ors, "Second-order ionospheric term in GPS: Implementation and impact on geodetic estimates," *Journal of Geophysical Research: Solid Earth*, 112(B8), 2007.

[21] M. List, S. Bremer, B. Rievers, and H. Selig, "Modelling of Solar Radiation Pressure Effects: Parameter Analysis for the MICROSCOPE Mission," *International Journal of Aerospace Engineering*, 2015.

[22] O. Montenbruck, P. Steigenberger, and U. Hugentobler, "Enhanced solar radiation pressure modeling for Galileo satellites," *Journal of Geodesy*, 89, pp. 283–297, 2015.